

Tropospheric HONO Distribution and Chemistry in the Southeast U.S.

Chunxiang Ye^{1,2}, Xianliang Zhou^{2,3}, Dennis Pu³, Jochen Stutz⁴, James Festa⁴, Max Spolaor⁴, Catalina Tsai⁴, Christopher Cantrell⁵, Roy L. Mauldin III^{5,6}, Andrew Weinheimer⁷, Rebecca S. Hornbrook⁷, Eric C. Apel⁷, Alex Guenther⁸, Lisa Kaser⁷, Bin Yuan⁹, Thomas Karl¹⁰, Julie Haggerty⁷, Samuel Hall⁷, Kirk Ullmann⁷, James Smith^{7,11}, John Ortega⁷

[1] State Key Joint Laboratory of Environmental Simulation and Pollution Control, College of Environmental Sciences and Engineering, the Key Joint Laboratory of Environment

[2] Wadsworth Center, New York State Department of Health, Albany, NY

[3] Department of Environmental Health Sciences, State University of New York, Albany, NY

[4] Department of Atmospheric and Oceanic Sciences, University of California, Los Angeles, CA

[5] Department of Atmospheric and Oceanic Sciences, University of Colorado-Boulder, Boulder Colorado

[6] Department of Physics, University of Helsinki, Helsinki, Finland

[7] National Center for Atmospheric Research, Boulder, Colorado

[8] Department of Earth System Science, University of California, Irvine, CA

[9] Institute for Environmental and Climate Research, Jinan University, Guangzhou, 511443

[10] Institute of Atmospheric and Cryospheric Sciences, University of Innsbruck, Innsbruck, Austria

[11] University of Eastern Finland, Kuopio, Finland

Correspondence to: Chunxiang Ye (c.ye@pku.ed.u.cn) and Xianliang Zhou (xianliang.zhou@health.ny.gov)

1 **Abstract**

2 Here we report the measurement results of nitrous acid (HONO) and a suite of relevant
3 parameters on the NCAR C-130 research aircraft in the Southeast U.S. during the NOMADSS
4 2013 summer field study. The daytime HONO concentration ranged from low parts per
5 trillion by volume (pptv) in the free troposphere (FT) to mostly within 5 - 15 pptv in the
6 background planetary boundary layer (PBL). There was no discernible vertical HONO
7 gradient above the lower flight altitude of 300 m in the PBL, and the transport of ground
8 surface HONO was found not a significant contributor to the tropospheric HONO budget. The
9 total *in situ* HONO source, mean (± 1 SD) was calculated $53 (\pm 21)$ pptv h⁻¹ during the day.
10 The upper limit contribution from NO_x-related reactions was $10 (\pm 5)$ pptv h⁻¹, and the
11 contribution from photolysis of particulate nitrate (pNO₃) was $38 (\pm 23)$ pptv h⁻¹, based on the
12 measured pNO₃ concentrations and the median pNO₃ photolysis rate constant of 2.0×10^{-4} s⁻¹
13 determined in laboratory using ambient aerosol samples. The photolysis of HONO contributed
14 to less than 10% of the primary OH source. However, a recycling NO_x source via pNO₃
15 photolysis was equivalent to $\sim 2.3 \times 10^{-6}$ mol m⁻² h⁻¹ in the air column within the PBL, a
16 considerable supplementary NO_x source in the low-NO_x background area. Up to several tens
17 pptv of HONO were observed in power plant and urban plumes during the day, mostly
18 produced *in situ* from precursors including NO_x and pNO₃. Finally, there was no observable
19 accumulation of HONO in the nocturnal residual layer and the nocturnal FT in the
20 background Southeast U.S., with an increase in HONO/NO_x ratio of $\leq 3 \times 10^{-4}$ hr⁻¹ after sunset.
21

22 1 Introduction

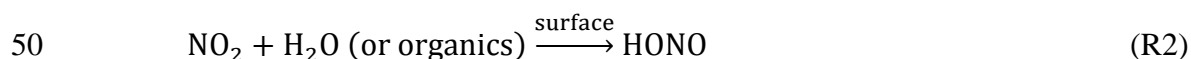
23 Extensive field studies at ground sites have shown that gas-phase nitrous acid (HONO)
24 exists at much higher levels than expected during the day, with a mixing ratio of HONO up to
25 several parts per billion by volume (ppbv) in the urban atmosphere (Acker et al., 2006;
26 Villena et al., 2011) and up to several hundred parts per trillion by volume (pptv) in rural
27 environments (Acker et al., 2006; Kleffmann et al., 2003; Zhang et al., 2009; Zhou et al.,
28 2002, 2011). At the observed concentrations, HONO photolysis (R1) becomes an important or
29 even a major OH primary source in both urban (Elshorbany et al., 2010; Villena et al., 2011)
30 and rural environments near the ground surface (Acker et al., 2006; He et al., 2006;
31 Kleffmann et al., 2003; Zhou et al., 2002, 2011).



33 The OH radical is responsible for the removal of primary pollutants, and plays a crucial role in
34 the formation of secondary pollutants, such as O₃ and aerosol (Finlayson-Pitts and Pitts,
35 2000), and thus HONO plays an important role in atmospheric chemistry.

36 The removal processes of HONO from the troposphere are relatively well understood,
37 including mainly photolysis, reaction with the OH radical and surface deposition. Photolysis
38 is the dominant sink for HONO during the day (Kleffmann et al., 2003; Oswald et al., 2015;
39 Zhang et al., 2009, 2012), and dry deposition is the major HONO loss pathway at night,
40 especially over wet surfaces (He et al., 2006; VandenBoer et al., 2015). However, HONO
41 sources in the planetary boundary layer (PBL) are numerous. HONO is directly emitted from
42 combustion processes, such as automobile emissions (Li et al., 2008b) and biomass burning
43 (Burling et al., 2010; Trentmann et al., 2003). Soil emission via nitrification or denitrification
44 is another source of HONO, which might be important in agriculture region (Maljanen et al.,
45 2013; Oswald et al., 2013; Su et al., 2011). Due to the relatively short photolytic lifetime of
46 HONO, in the order of 10 min around summer noontime, the impacts of the direct emission
47 on HONO distribution and chemistry is highly localized and limited to the source region.

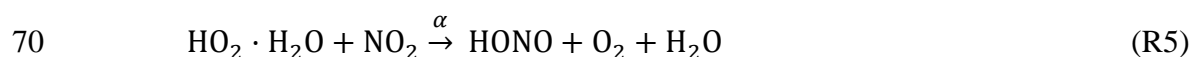
48 HONO is a unique species that is produced through heterogeneous reactions of
49 different precursors, such as NO₂ and HNO₃, on surfaces (R2 - R3):



52 Heterogeneous reactions of NO₂ with organics (R2) on the surfaces have been found to be
53 greatly accelerated by sunlight through photosensitization (George et al., 2005; Kleffmann,

54 2007; Stemmler et al., 2006, 2007) and these reactions on ground surfaces are likely the major
55 daytime HONO source in urban environments (Acker et al., 2006; Villena et al., 2011; Wong
56 et al., 2011). Laboratory studies have confirmed that HNO₃ undergoes photolysis in sunlight
57 at rates 2 - 3 orders of magnitude greater on the surface than in the gas phase (Baergen and
58 Donaldson, 2013; Du and Zhu, 2011; Ye et al., 2016a, b; Zhou et al., 2003; Zhu et al., 2008),
59 producing NO_x and HONO. In low-NO_x environments, photolysis of nitric acid/nitrate
60 deposited on the surface has been proposed to be the major daytime HONO source near the
61 ground surface (Ye et al., 2016b; Zhou et al., 2003, 2011).

62 Several processes within an air mass may lead to volume, or *in situ*, production of
63 HONO. The OH+NO reaction (R-1) in the gas phase may be a significant HONO source in
64 high NO_x and photochemically reactive atmospheres (Kleffmann, 2007; Neuman et al., 2016;
65 Villena et al., 2011), but becomes negligible in low-NO_x environments (Li et al., 2014; Ye et
66 al., 2016b). Two additional gas-phase reactions have been proposed to produce HONO within
67 the air column: between excited NO₂ (NO₂^{*}) and water vapor (R4) (Li et al., 2008a), and
68 between NO₂ and the hydroperoxyl-water complex (HO₂·H₂O) (R5) (Li et al., 2014):



71 However, further laboratory evidence suggests that reaction (R4) is too slow to be important
72 (Carr et al., 2009; Wong et al., 2011). And recent airborne observations have demonstrated
73 that the HONO yield (α) from reaction (R5) is less than 0.03 (Ye et al., 2015). Heterogeneous
74 reactions of NO₂ (R2) on aerosol surfaces and photolysis of particulate nitrate (pNO₃)
75 associated with aerosol particles similar to (R3) also contribute *in situ* HONO production in
76 the air column.

77 Most HONO measurements have been made at ground stations. The observed HONO
78 concentrations reported in the literature represent the HONO levels in the lower PBL under
79 the significant but varying influence of ground surface processes. Thus, it is difficult to
80 distinguish the ground surface HONO sources from the *in situ* HONO sources. Measurements
81 of vertical HONO concentration profiles and HONO fluxes have suggested that ground
82 surfaces can be major HONO sources for the overlying atmosphere in many cases (He et al.,
83 2006; Kleffmann et al., 2003; Stutz et al., 2002; Zhou et al., 2011; VandenBoer et al., 2013;
84 Young et al., 2012), but not in some other cases (Villena et al., 2011). A recent HONO flux
85 measurement has suggested that the HONO source from the forest canopy contributed ~ 60%
86 of the measured HONO budget at the measurement height of 11 m above the forest canopy,

87 and the *in situ* HONO production contributed the remaining ~ 40% (Zhou et al., 2011).
88 Similarly, observational and modeling studies implied a presence of a volume HONO source
89 at 130-m altitude above Houston, TX (Wong et al., 2012, 2013). The relative importance of *in*
90 *situ* HONO production would be expected to increase with altitude due to decreasing
91 influence of the ground surface, at least during the day. Airborne measurements in the air
92 mass above the altitude influenced directly by ground HONO sources should provide more
93 direct and quantitative evidence for *in situ* HONO production in the troposphere. Indeed, the
94 limited number of airborne measurements available have shown that HONO exists not only in
95 substantial amounts in combustion and urban plumes (Neuman et al., 2016) but also
96 throughout the troposphere (Li et al., 2014; Ye et al., 2015; Zhang et al., 2009).

97 Here we report airborne HONO measurement results and findings from five research
98 flights in the Southeast U.S. during the NOMADSS (Nitrogen, Oxidants, Mercury and
99 Aerosol Distributions, Sources and Sinks) 2013 summer field campaign aboard the
100 NSF/NCAR C-130 research aircraft.

101 **2 Experimental**

102 NOMADSS was an airborne field study under the “umbrella” of SAS (Southeast
103 Atmosphere Study). It consisted of nineteen research flights on board the NSF/NCAR C-130
104 aircraft from June 1, 2013 to July 15, 2013. Parameters observed included HONO, HNO₃,
105 particulate nitrate, NO_x, O₃, BrO, OH radicals, HO₂ radicals, RO₂ radicals, aerosol surface
106 area densities (size <1 μm), VOCs, photolysis frequencies, and other meteorology parameters.
107 Table 1 summarizes the instrumentation, time resolution, detection limit, accuracy, and
108 references for the measurements. The results from five out of nineteen flights are presented
109 here to discuss vertical HONO distribution and HONO chemistry in the Southeast U.S. The
110 flight tracks are shown in Figure 1.

111 **2.1 LPAP measurements of HONO and pNO₃**

112 HONO was measured by two long-path absorption photometric (LPAP) systems based
113 on the Griess-Saltzman reaction (Zhang et al., 2012; Ye et al., 2016b). Briefly, ambient air
114 was first brought into the aircraft through a heated PFA inlet, with a residence time of 0.14 s.
115 HONO was scrubbed using de-ionized (DI) water in two 10-turn glass coil samplers and the
116 collected nitrite was then derivatized with 5 mM sulfanilamide (SA) and 0.5 mM N-(1-
117 Naphthyl)-ethylene-diamine (NED) in 40 mM HCl, to form an azo dye. The azo dye was then

118 detected by light absorption at 540 nm using an 4-channel optic fiber spectrometer (LEDSpec,
119 WPI) with two 1-m liquid waveguide capillary flow cells (WPI). Each LPAP system ran a 30-
120 min measurement and zero cycle, with 20 min sampling ambient air and 10 min sampling
121 “zero-HONO” air for baseline correction, and with a 15-min time offset between the two
122 sampling cycles. The combination of the data from the two systems provides continues
123 HONO concentration measurement. The “zero-HONO” air was generated by directing the
124 sample stream through a Na₂CO₃-coated denuder to remove HONO while allowing most of
125 interfering species (NO_x, PAN, and particulate nitrite) to pass through . The absorbance
126 signals were sampled at a rate of 1 Hz, and were averaged into 1-min or 3-min data for
127 analysis.

128 Interference from NO_x, PAN, and particulate nitrite was corrected by subtracting the
129 baseline from the ambient air signal. Due to the low collecting efficiency of these interfering
130 species in the sampling coil and their low concentrations, the combined interference was
131 estimated to be less than 10% of the total signal. Potential interference from peroxyacetic acid
132 (HO₂NO₂) was suppressed by heating the PFA sampling line to 50 °C. The HO₂NO₂ steady
133 state concentration ([HO₂NO₂]_{SS}) was estimated to be less than 1 pptv at temperatures of 20 -
134 30 °C in the background PBL (Gierczak et al., 2005), and thus interference from HO₂NO₂ was
135 negligible. Whereas in power plant and urban plumes in the PBL or biomass burning plumes
136 in the upper free troposphere (FT), HO₂NO₂ interference was not negligible and thus a
137 correction for HONO measurement was made. An upper-limit HO₂NO₂ response efficiency
138 was estimated to be 0.2 for our HONO measurement systems. The estimation was made from
139 the lowest ratio of the measured HONO to the corresponding [HO₂NO₂]_{SS} in cold air masses
140 at high altitude, assuming no HONO existed. HONO concentration were then corrected by
141 subtracting a term of “0.2 × [HO₂NO₂]_{SS}”. The correction was below 10% of the measured
142 HONO concentrations in the PBL plumes. However, there may be over-corrections in the cold
143 free troposphere.

144 The lower detection limit of LPAP-HONO measurement was estimated to be ≤1 pptv,
145 based on 3 times the standard deviation of the zero air signal (N >10). An overall uncertainty
146 of ±(1 + 0.2 [HONO]) pptv was estimated, combining the uncertainties in signal acquisition
147 and processing, air and liquid flow rates, standard preparation, and baseline correction. The
148 accuracy of HONO measurements was confirmed by comparison with a limb-scanning
149 Differential Optical Absorption Spectroscopy (DOAS) (Platt and Stutz, 2008). The agreement
150 between these two instruments was very good in wide power plant plumes where HONO

151 mixing ratios significantly exceeded the detection limits of both instruments (Ye et al.,
152 2016b).

153 Particulate nitrate (pNO_3) was quantitatively collected with a frit disc sampler after a
154 NaCl-coated denuder to remove HNO_3 (Huang et al., 2002). The collected nitrate was reduced
155 to nitrite by a Cd column, and determined using a LPAP system (Zhang et al., 2012). “Zero-
156 pNO_3 ” air was generated to establish measurement baselines for pNO_3 by passing the ambient
157 air through a Teflon filter to remove aerosol particles and then a NaCl-coated denuder to
158 remove HNO_3 before reaching the sampling unit of LPAP. Potential interferences from
159 HONO, NO_x and PAN were corrected by subtracting the baselines from the ambient air
160 signals. The lower detection limit of pNO_3 was estimated to be 2 pptv, based on 3 times the
161 standard deviation of the zero air signal ($N > 10$). An overall uncertainty of $\pm(2 + 0.3 [\text{pNO}_3])$
162 pptv was estimated.

163 Noisy baselines were observed when the C-130 was flying in the clouds, due to the
164 sampling of cloud droplets by our sampling systems. Because of the lack of a valid way to
165 correct for this interference, all in-cloud measurement data of HONO and pNO_3 have been
166 excluded from the data analysis.

167 **2.2 Supporting measurements**

168 The mixing ratios of a large number of non-methane organic compounds (NMOCs) were
169 measured by Trace Organic Gas Analyzer (TOGA) (Hornbrook et al., 2011a) and Proton-
170 transfer-reaction mass spectrometry (PTR-MS) (Karl et al., 2003; de Gouw and Warneke,
171 2007). The surface area density of fine particles was obtained by the measurement of a
172 Scanning Mobility Particle Sizer (SMPS), under the assumption of preface sphere of aerosol
173 particle. The photolysis frequencies were determined by a Charged-coupled device Actinic
174 Flux Spectroradiometer instrument (CAFS) (Shetter et al., 2002). The mixing ratios of HO_x
175 and RO_2 radicals were measured by a method based on selected-ion chemical-ionization mass
176 spectrometry (SICIMS) (Hornbrook et al., 2011b; Mauldin et al., 2010). The mixing ratios of
177 ozone and NO_x were measured by chemiluminescence instruments (Ridley et al., 2004).
178 Meteorology parameters were provided by state parameter measurements on board the C-130.

179 **3 Results and Discussion**

180 **3.1 General data description**

181 Figure 2 shows the time series of HONO, NO_x, pNO₃ concentrations and the measurement
182 altitude for five selected research flights in the Southeast U.S. during the NOMADSS 2013
183 summer field study. Research flight (RF) #4, RF #5 and RF #17 are race track flights in the
184 background terrestrial areas designed to establish HONO distribution and explore HONO
185 chemistry in background air masses. RF #11 is a race track flight designed to intercept plumes
186 from local power plants and urban areas and explore HONO chemistry therein. All four flights
187 were conducted in the daytime, roughly from 14:00 to 22:00 UTC (10:00 to 18:00 EDT). RF
188 #18 is a race track flight conducted from 20:30 on July 12th to 03:30 on July 13th UTC (16:30
189 to 23:30 on July 12th, 2013 EDT), aiming to study the potential night-time HONO
190 accumulation both in the PBL and the FT.

191 Table 2 summarizes the data statistics for HONO, NO_x and pNO₃ measurements in the
192 PBL and the FT, and Figure 3 shows composite vertical distributions of HONO, NO_x and
193 pNO₃ concentrations from the five flights in the Southeast U.S. during the NOMADSS 2013
194 summer field study. HONO, NO_x and pNO₃ concentrations show horizontal gradients in every
195 race track flight and vary in different race track flights, reflecting the inhomogeneity of air
196 masses in the region. However, there was no significant vertical gradient in HONO, NO_x and
197 pNO₃ concentrations, which will be further discussed below. Except in a few power plant
198 plumes and urban plumes mostly encountered in RF #11, most of the data is representative of
199 background terrestrial air masses. The range of the mixing ratio of HONO is 3.1 – 34.4 pptv.
200 The mean ($\pm 1SD$) and median values of HONO concentration are 5.6 (± 3.4) pptv and 4.2 pptv
201 in the FT, and 11.2 (± 4.3) pptv and 10.3 pptv in the PBL. HONO levels at ~ 4 pptv are
202 typically found in the background FT, but high HONO concentrations up to 15.2 pptv are also
203 observed in the elevated biomass burning plumes. HONO levels at ~ 11 pptv are
204 representative of background conditions in the PBL. High HONO levels up to 34.4 pptv are
205 observed in the power plant plumes and urban plumes in RF #11 (see section 3.4) and RF #
206 17. These measured HONO values are consistent with the range of 4 – 74 pptv in the
207 troposphere over Northern Michigan (Zhang et al., 2009), but are significantly lower than 100
208 - 150 pptv in the morning residual layer over an industrial region of Northern Italy (Li et al.,
209 2014), where the levels of HONO precursors, such as NO_x and pNO₃, were much higher. The
210 HONO concentrations were also consistent with the levels reported for the same region during
211 the Southeast Nexus Experiment on the NOAA WP-3D aircraft (Neuman et al., 2016), that is,
212 “indistinguishable from zero within the 15 parts per trillion by volume measurement

213 uncertainty” in the background air and up to 150 pptv in the power plant plumes during the
214 day. The lower HONO concentrations measured in the power plant plumes in this study than
215 the daytime values reported by Neuman et al (2016) probably reflects greater dilution of
216 smaller plumes encountered by the C-130 than by the WP-3D, as indicated by much lower
217 NO_x levels observed, up to 1.8 ppbv vs up to 60 ppbv.

218 The range of the mixing ratio of NO_x is from several pptv to around 1.8 ppbv. The
219 mean ($\pm 1SD$) and median values of NO_x concentration are 94 (± 53) pptv and 92 pptv in the
220 FT, and 316 (± 182) pptv and 279 pptv in the PBL. The mixing ratios of NO_x are mostly
221 between 50 - 150 pptv in the background conditions in the FT and between 200 - 500 pptv in
222 the background conditions in the PBL. Similar to HONO, high values of NO_x also occur in the
223 urban and power plant plumes in the PBL (up to 1.8 ppbv) and in the biomass burning plumes
224 in the FT (up to 0.6 ppbv).

225 Fewer measurement data points are available for pNO₃, compared to those for NO_x
226 and HONO, due to air bubble formation in the flow cell of the pNO₃ system, especially at
227 high altitudes. The range of the mixing ratio of pNO₃ is from 3 pptv to 186 pptv, with the
228 mean ($\pm 1SD$) and median values of 35 (± 39) pptv and 15 pptv in the FT, and 76 (± 45) pptv
229 and 66 pptv in the PBL. The pNO₃ levels were highly variable in both the FT and the PBL. In
230 the FT, the pNO₃ levels were often under 10 pptv, but high concentrations up to 179 pptv were
231 also observed in elevated biomass burning plumes. In the PBL, high pNO₃ levels were
232 sometimes observed in relative clean conditions; whereas, low pNO₃ levels were observed in
233 high HONO and NO_x power plant plumes. Both the N(V) level (= [HNO₃] + [pNO₃]) and the
234 partitioning between HNO₃ and pNO₃ seem to play roles in determining the pNO₃ level.

235 **3.2 HONO contribution from ground-level sources**

236 There are several ground-level HONO sources that may contribute to the HONO
237 budget in the overlying atmosphere. They include anthropogenic sources, such as power plant
238 and automobile emissions (Li et al., 2008b; Neuman et al., 2016), and natural processes, such
239 as soil emission (Maljanen et al., 2013; Oswald et al., 2013; Su et al., 2011), heterogeneous
240 reactions of NO₂ (Acker et al., 2006; George et al., 2005; Ndour et al., 2008, 2009; Ramazan
241 et al., 2006) and surface HNO₃ photolysis (Ye et al., 2016b; Zhou et al., 2003,2011). Since
242 HONO photolytic lifetime is relatively short, e.g. 8 - 16 min in RF #4, RF #5, RF #11 and RF
243 #17, a steep negative vertical gradient of HONO concentration would be expected if a
244 significant contribution originated from the ground. The lack of a significant vertical gradient

245 in the measured HONO concentrations (Fig. 3a) thus suggests that the ground contribution is
246 either limited to the shallow layer of the boundary layer near the ground, below the C-130
247 lowest flight altitude of 300 m, or small relative to the *in situ* production of HONO in the air
248 column (Ye et al., 2017).

249 To further examine the potential HONO contribution from the ground sources, vertical
250 profiles of HONO, NO_x, and pNO₃, are compared with those of potential temperature (K) and
251 isoprene measured, for example, in the first race-track of RF#4 from 11:00 – 12:15 LT (Fig.
252 4). The PBL height (*H*) was ~ 1200 m as indicated by the constant potential temperature (Fig.
253 4e). The vertical distribution of isoprene originating from the ground can be expressed with
254 the following equation (Eq.1):

$$255 \quad \ln\left(\frac{C}{C_0}\right) = -\frac{k\tau}{H}h = -\frac{h}{h^*} \quad (\text{Eq. 1})$$

256 where *C*₀ and *C* are its concentrations near the ground and at the altitude *h*, *k* is the pseudo-
257 first order degradation rate constant, *τ* is the average mixing time in the PBL, and *h** (=
258 *H*/(*kτ*)) is its characteristic transport height within one degradation lifetime of isoprene.
259 According to the best fit of (Eq.1) to the observed isoprene data (Fig. 4d), its characteristic
260 transport height *h** is estimated 692 m for isoprene. Assuming isoprene is mainly oxidized by
261 the OH radical whose average concentration is estimated at 3 × 10⁶ mole cm⁻³ in the PBL
262 (Kaser et al., 2015), the pseudo-first order degradation rate constant of ~ 3.0 × 10⁻⁴ s⁻¹ (or the
263 degradation rate of ~ 0.93 h⁻¹) is determined for isoprene. Based on a boundary layer height of
264 ~1.2 km (Fig. 4e), an average PBL mixing time *τ* is estimated to be ~1.6 h between 11:00 –
265 12:15 LT of RF #4. With a photolytic lifetime of ~ 11 min for HONO, about 11% of the
266 HONO originated from the ground level is expected to reach the altitude of 300 m, the lowest
267 flight altitude of the C-130 aircraft between 11:00 – 12:15 LT in RF #4. The vertical mixing
268 of the PBL is enhanced from the morning to the afternoon, as the ground surface is heated by
269 solar radiation gradually during the day. The average mixing time in the PBL is reduced from
270 ~ 3 h in the morning, to ~ 1.5 h around noontime, and to ~ 30 min in the afternoon,
271 determined from isoprene gradients from RF #4, #5 and #17. About 50% of the ground
272 emitted HONO could survive and be transported to lower measurement altitudes. Again, if
273 this ground source contribution was significant, the HONO concentration profile should
274 exhibit a significant gradient, probably more pronounced than that of isoprene due to its
275 shorter lifetime. The lack of such a vertical HONO gradient in the measured HONO
276 concentration profiles (Fig. 3a) suggests that the contribution from ground HONO sources to
277 the observed HONO concentrations in the PBL above 300 m is insignificant.

278 The NO_x level was ≤ 0.5 ppbv in the PBL over the Southeast U.S. (Figure 2),
 279 excluding the power plant plumes. Based on an upper limit HONO/NO_x ratio of 0.05 for
 280 urban atmosphere at ground level (Villena et al., 2011), the initial HONO concentration would
 281 be ≤ 25 pptv in the source air mass on the ground level. With a transport time of ≥ 0.5 h, i.e.,
 282 ≥ 3 times of the HONO photolysis lifetime, the contribution from the ground HONO source
 283 would be ≤ 1 pptv. This analysis supports the conclusion that contribution of surface HONO
 284 source to the PBL HONO budget is insignificant.

285 3.3 Daytime HONO chemistry in low NO_x areas

286 After removing the data measured in the urban and power plant plumes, the daytime HONO
 287 concentrations are within the range of 5 - 15 pptv throughout the PBL in the background
 288 terrestrial areas in the five race-track research flights. Photolysis is the dominant sink for
 289 HONO, with a photolysis lifetime of 8 - 16 min during these four daytime flights (RF #4, RF
 290 #5, RF #11, and RF #17). Therefore, there must be a significant volume HONO source, up to
 291 173 pptv h⁻¹, within the air mass to sustain the observed HONO concentrations.

292 Both NO_x and pNO₃ are potential HONO precursors in the air column. While HONO
 293 correlates moderately with NO_x (r² = 0.45, Fig S1), it only weakly correlates with pNO₃ (R² =
 294 0.17). It appears at first that NO_x is a more important HONO precursor than pNO₃. However,
 295 the detailed analysis below suggests that NO_x is only a minor precursor to the observed
 296 HONO, and photolysis of pNO₃ is the major *in situ* HONO source.

297 The upper limit of photo-stationary state HONO concentration ([HONO]_{pss}) was
 298 calculated using Equation 2 that takes into account all the known HONO source contributions
 299 from NO_x-related reactions, including gaseous reactions of OH and NO (R-1), excited NO₂
 300 (NO₂^{*}) and water vapor (R4) (Carr et al., 2009; Li et al., 2008a), NO₂ and the hydroperoxyl-
 301 water complex (HO₂·H₂O) with an upper limit HONO yield of 3% (R5a)(Li et al., 2014; Ye et
 302 al., 2015), and heterogeneous reaction of NO₂ on aerosol surfaces (R2) using an upper limit
 303 uptake coefficient of 10⁻⁴ reported in the literature (George et al., 2005; Monge et al., 2010;
 304 Ndour et al., 2008, 2009; Stemmler et al., 2006, 2007):

$$305 \quad [\text{HONO}]_{pss} = \frac{k_{-1}[\text{NO}][\text{OH}] + k_4[\text{NO}_2^*][\text{H}_2\text{O}] + \alpha k_5[\text{NO}_2][\text{HO}_2 \cdot \text{H}_2\text{O}] + k_2 S_{aerosol}[\text{NO}_2]}{J_{\text{HONO}} + k_{\text{OH-HONO}}[\text{OH}]} \quad (\text{Eq. 2})$$

306 where $S_{aerosol}$ is the aerosol surface area density. It should be noted that the upper limit values
 307 of rate constants were used in the calculation to avoid the underestimation of [HONO]_{pss}
 308 value. Under typical daytime conditions in the PBL with the median measured values of
 309 reactants, the upper limit [HONO]_{pss} value is less than 2 pptv, much lower than the median

310 measured HONO concentration of ~ 11 pptv. Figure 5a shows the relationship ($r^2 = 0.40$)
 311 between the photolytic HONO loss rate with the sum of HONO production rates from all the
 312 NO_x -related reactions calculated with upper-limit reaction rate constants. A slope of about
 313 0.19 indicates that the contribution from these NO_x -related reactions to the volume HONO
 314 source is minor in the background troposphere, despite the good correlation between HONO
 315 and NO_x .

316 Photolysis of HNO_3 on surfaces has been found to proceed at a much higher rate than
 317 in the gas phase (Baergen and Donaldson, 2013; Du and Zhu, 2011; Ramazan et al., 2004; Ye
 318 et al., 2016b; Zhou et al., 2003; Zhu et al., 2008), with HONO as the major product on
 319 environmental surfaces (Ye et al., 2016a, 2017). Furthermore, photolysis of particulate nitrate
 320 has been found to be the major daytime HONO source in the marine boundary layer (Ye et al.,
 321 2016b). To examine the role of particulate nitrate as a potential HONO source in the
 322 troposphere, aerosol samples were collected and used in the light-exposure experiments to
 323 determine the photolysis rate constants for particulate nitrate in the laboratory. The
 324 determined pNO_3 photolysis rate constant ($J_{\text{pNO}_3}^N$) varies over a wide range, from $8.3 \times 10^{-5} \text{ s}^{-1}$
 325 to $3.1 \times 10^{-4} \text{ s}^{-1}$, with a median of $2.0 \times 10^{-4} \text{ s}^{-1}$ and a mean ($\pm 1 \text{ SD}$) of $1.9 (\pm 1.2) \times 10^{-4} \text{ s}^{-1}$, when
 326 normalized to tropical noontime conditions at ground level (solar zenith angle = 0°), and the
 327 average HONO to NO_2 relative yield is 2.0 (Ye et al., 2017). Figure 6b shows the relationship
 328 between the photolytic HONO loss rate ($J_{\text{HONO}} \times [\text{HONO}]$) and the volume HONO production
 329 rates from pNO_3 photolysis ($2/3 \times J_{\text{HNO}_3} \times [\text{pNO}_3]$). The median $J_{\text{pNO}_3}^N$ of $\sim 2.0 \times 10^{-4} \text{ s}^{-1}$ was used
 330 to calculate the ambient J_{pNO_3} by scaling to J_{HNO_3} :

$$331 \quad J_{\text{pNO}_3} = J_{\text{pNO}_3}^N \times \frac{J_{\text{HNO}_3}}{7.0 \times 10^{-7} \text{ s}^{-1}} \quad (\text{Eq. 3}),$$

332 where J_{HNO_3} is the photolysis rate constant of gas-phase HNO_3 calculated from light intensity
 333 measurement on the C-130 aircraft, and $7.0 \times 10^{-7} \text{ s}^{-1}$ is the photolysis rate constant of gas-
 334 phase HNO_3 under the tropical noontime condition at ground level (solar zenith angle = 0°). A
 335 slope of 0.69 can be derived from Figure 5b, suggesting that pNO_3 photolysis is the major
 336 volume HONO source. However, the r^2 of 0.34 is not as strong as expected from pNO_3
 337 photolysis being the major volume HONO source. It may be in part due to the use of a single
 338 median $J_{\text{pNO}_3}^N$ value of $\sim 2.0 \times 10^{-4} \text{ s}^{-1}$ in the calculations of the ambient J_{pNO_3} and the
 339 production rates of HONO in Figure 5b; the actual $J_{\text{pNO}_3}^N$ values are highly variable, ranging
 340 from $8.3 \times 10^{-5} \text{ s}^{-1}$ to $3.1 \times 10^{-4} \text{ s}^{-1}$ (Ye et al., 2017). HONO source contribution from

341 particulate nitrate photolysis in Figure 5b are thus estimates of the *in situ* HONO production
342 rates from pNO₃ photolysis in different air masses.

343 HONO photolysis has been found to be an important or even a major OH primary
344 source in the atmosphere near the ground surface (Elshorbany et al., 2010; He et al., 2006;
345 Kleffmann et al., 2003; Villena et al., 2011; Zhou et al., 2011). However, HONO is not a
346 significant daytime OH precursor in the background troposphere away from the ground
347 surface. Based on the measurement results in this study, the mean (\pm SD) contribution of
348 HONO photolysis to the OH source budget is 53 (\pm 21) pptv h⁻¹ in the PBL and 44 (\pm 26) pptv
349 h⁻¹ in the FT (Table S1), respectively, less than 10% of the OH production contributed by O₃
350 photolysis. Since HONO is mainly produced from photolysis of particulate nitrate, it becomes
351 an important intermediate product of a photochemical renoxification process recycling nitric
352 acid and nitrate back to NO_x. The regenerating rate of NO_x of about 38 (\pm 23) pptv h⁻¹ via
353 pNO₃ photolysis (Table S1) is equivalent to an air column NO_x source of $\sim 2.3 \times 10^{-6}$ mol m⁻²
354 h⁻¹ in the 1.5- km PBL, a considerable supplementary NO_x source in the low-NO_x background
355 area.

356 It should be pointed out that particulate nitrate is in a dynamic equilibrium with gas-
357 phase HNO₃, the later accounts for a larger (or even dominant) fraction of total nitrate
358 (pNO₃+HNO₃) and is photochemically inert. The overall photolysis of pNO₃+HNO₃ would be
359 much slower than indicated by J_{pNO_3} . In addition, oxidation of NO_x via several reactions will
360 replenish the pNO₃+HNO₃ reservoir. The results reported here and in earlier papers (Reed et
361 al., 2017; Ye et al., 2016a) suggest that there is a rapid cycling in reactive nitrogen species in
362 the low-NO_x atmosphere, sustaining the observed levels of HONO and pNO₃.

363 **3.4 HONO chemistry in plumes**

364 One of the objectives of RF #11 was to study the chemistry of HONO in urban and coal fired
365 power plant plumes. The arrows and corresponding labels in Figure 2 indicate the urban
366 plumes (U1-U3) and power plant plumes (P1-P4). CO and benzene were used to identify
367 influence from urban plumes, SO₂ to identify influence from power plant plumes, and
368 acetonitrile to identify the influence of biomass burning plumes (Fig. S2). The plumes U1-U3
369 were identified as urban plumes from cities of Birmingham (U1, U3) and Montgomery (U2)
370 in Alabama, respectively, and plumes P1-P4 were identified as power plant plumes from
371 power plants in Monroe county (P1-P3) and Putman county(P4) in Georgia, respectively. The
372 influence of biomass burning plumes was negligible as acetonitrile concentration was low and

373 stable. The power plant plumes were generated from high-intensity point sources, and thus
374 had features of narrow but high peaks of both HONO and NO_x concentrations in the time-
375 series plots (Figs. 2, 6 & S2). In contrast, the urban plumes were generated from area sources
376 and thus were shown as broad peaks of HONO and NO_x in the time-series plot with low levels
377 of NO_x (mostly below 500 pptv) (Figs. 2, 6 & S2). There were a few sharp but small NO_x
378 peaks within the broad urban plumes, reflecting the contributions of some point sources in the
379 urban areas. The observed HONO/NO_x ratio was 0.019 (\pm 0.004) in the power plant plumes
380 (e.g., P4) and 0.057 (\pm 0.0019) in urban plumes, significantly higher than the typical
381 HONO/NO_x emission ratio of \sim 0.002 in the fresh power plant plumes (Neuman et al., 2016)
382 and \leq 0.01 in automobile exhaust (Kurtenbach et al., 2001; Li et al., 2008b). The elevated
383 HONO/NO_x ratios observed in the plumes suggest that the observed HONO was mostly
384 produced from precursors within the air mass during the transport. Based on the distances
385 between measurement locations from the power plants or the centres of urban areas and wind
386 speed, the transport times of these plumes were estimated to be \geq 1 h, \sim 5 times longer than
387 HONO photolysis lifetime of 8 - 16 min, again suggesting that most of the observed HONO in
388 the plumes was produced *in situ* within the air masses.

389 Figure 6 shows the time-series plot of HONO budgets within the air masses sampled
390 by the C-130 aircraft during flight RF# 11, comparing its photolysis loss rate with its
391 production rates from pNO₃ photolysis and from all the NO_x-related reactions combined.
392 Photolysis of particulate nitrate appears to be the major volume HONO source in all urban
393 plumes and in most of the power plant plumes except for plume P4 observed here. NO_x was
394 generally more important as a HONO precursor in the power plant plumes than in the urban
395 plumes and in low-NO_x background air masses, due to higher levels of NO_x (up to 1.8 ppb in
396 Figs. 2c and S2), OH radical and aerosol surface density. For example, all the NO_x-related
397 reactions combined contributed up to 52% of the total volume HONO source required to
398 sustain the observed HONO concentration in plume P4 (Fig. 6). In fresh and larger power
399 plant plumes encountered during the RF #7 to Ohio River Valley (X. Zhou, unpublished data),
400 over 20 ppb NO_x was detected, and the NO_x-related reactions, mainly the NO+OH reaction,
401 were found to account for almost all the required HONO source strength to sustain the
402 observed HONO, in agreement with Neuman et al. (2016). The power plant plumes undergo
403 rapid physical and photochemical evolution during the day, such as dilution and NO_x-to-
404 HNO₃ conversion. Thus, the relative contributions from NO_x-related reactions and particulate
405 nitrate photolysis as HONO sources change rapidly as the plumes age.

406 3.5 Night-time HONO chemistry

407 Nighttime HONO accumulation has been widely observed at the ground level (Kleffmann et
408 al., 2003; Oswald et al., 2015; 2008; Stutz et al., 2002, 2010; VandenBoer et al., 2013, 2014,
409 2015), contributed by various anthropogenic and natural HONO sources on the ground. The
410 main objective of RF #18 was to study the night-time HONO evolution in both the nocturnal
411 residual layer and the nocturnal FT. After sunset, the surface cooling promotes the formations
412 of a inversion layer near the ground surface and a nocturnal residual layer above; the
413 contribution from ground HONO sources then becomes negligible to the air masses beyond
414 the surface inversion layer. Meanwhile, no effective HONO sinks, such as photolysis,
415 oxidation by OH and dry deposition, exist in the nocturnal residual layer. Thus the HONO
416 accumulation, if any, is a net contribution from dark heterogeneous NO₂ reaction on aerosol
417 surfaces (R2).

418 The C-130 flew in an elongated race track pattern along a north-south direction, about
419 140 km from Nashville, TN (Fig. 1), alternating between the PBL (1200 m) and the FT (2500
420 m), from late afternoon to midnight local time (Fig. 2). In the FT, HONO and NO_x
421 concentrations were relatively stable throughout the afternoon and the night, staying around 4
422 ppt and 90 pptv respectively. The lack of night-time HONO accumulation is expected from
423 the low levels of HONO precursors, mostly NO₂, and surface area of aerosol particles in the
424 FT (Fig. 2).

425 The conditions in the PBL were far more variable and complicated. There were strong
426 horizontal gradients of NO_x, pNO₃ and HONO in the PBL, with higher concentrations at the
427 southern end and lower concentrations at the northern end of the flight track. Back-trajectory
428 analysis using NOAA's HYSPLIT model (Stein et al., 2015) indicates that the encountered air
429 masses in the PBL at the southern end passed over Nashville, about 140 km northeast of the
430 sample area, with a transport time of about 6 h (Fig. S3a), while the air masses at the northern
431 end stayed to north of Nashville (Fig. S3b). Therefore, the anthropogenic emissions from the
432 metropolitan area of Nashville contributed to the higher concentrations of pollutants observed
433 at the southern end of the flight track. There were also trends of increasing concentrations of
434 NO_x, pNO₃ and HONO with time after the sunset (Fig. 2). This was probably a result of less
435 dispersion and dilution of anthropogenic pollutants, including NO_x, as the PBL became more
436 stable after sunset. Furthermore, as time progressed from late afternoon into evening and

437 night, the air masses were less photochemically aged during the transport from the source
 438 areas, due to the decreasing solar light intensity and shorter solar light exposure time.

439 Because of the large spatial and temporal variations in the concentrations of HONO and
 440 its precursors in the PLB (Fig. 2), it is difficult to directly evaluate the nighttime HONO
 441 accumulation from HONO measurements alone. The concentration ratio of HONO and its
 442 dominant nighttime precursor, NO₂, can be used as an indicator of nighttime HONO
 443 accumulation. As the air masses at measurement altitude of 1200 m decoupled from the
 444 ground-level processes after sunset, the HONO production ($P(\text{HONO})$) from heterogeneous
 445 NO₂ reaction (R2) on aerosol surface becomes the only HONO source, and can be expressed
 446 by the following equations (Eq. 4 and Eq. 5):

$$447 \quad P(\text{HONO}) = \frac{1}{4} \times \left[\frac{s}{v} \right] \times \sqrt{\frac{8RT}{\pi M}} \times \gamma \times [\text{NO}_2] \quad (\text{Eq.4})$$

$$448 \quad \frac{P(\text{HONO})}{[\text{NO}_2]} = \frac{1}{4} \times \left[\frac{s}{v} \right] \times \sqrt{\frac{8RT}{\pi M}} \times \gamma \quad (\text{Eq.5})$$

449 where $\left[\frac{s}{v} \right]$ is the specific aerosol surface area density, R is the gas constant, K the absolute
 450 temperature, M the molecular weight of NO₂, and γ is the dark uptake coefficient of NO₂
 451 leading to HONO production. The NO₂-normalized HONO accumulation over time, $\Delta \frac{[\text{HONO}]}{[\text{NO}_2]}$,
 452 can then be calculated by equation (Eq. 6):

$$453 \quad \Delta \frac{[\text{HONO}]}{[\text{NO}_2]} \sim \frac{1}{4} \times \left[\frac{s}{v} \right] \times \sqrt{\frac{8RT}{\pi M}} \times \gamma \times \Delta t \quad (\text{Eq. 6})$$

454 Assuming a dark uptake coefficient γ of 1×10^{-5} of NO₂ on aerosol (George et al., 2005;
 455 Monge et al., 2010; Ndour et al., 2008; Stemmler et al., 2006, 2007) with a $\left[\frac{s}{v} \right]$ value of $\sim 10^{-4}$
 456 m⁻¹, a relative HONO accumulation rate, $\Delta \frac{[\text{HONO}]}{[\text{NO}_2]} / \Delta t$ of $\sim 0.0003 \text{ h}^{-1}$ is estimated using the
 457 equation (Eq. 6), equivalent to a HONO accumulation of 0.13 pptv hr⁻¹ at a constant NO₂
 458 concentration of 400 pptv. Such a low HONO accumulation rate is below our measurement
 459 detection limit. Indeed, the calculated HONO to the NO_x ratio using the measurement data
 460 stayed almost unchanged with time (Fig. 7), well within the observational variability after the
 461 sunset, suggesting no significant volume production of HONO in the nocturnal boundary
 462 layer.

463 **4 Conclusions**

464 Substantial levels of HONO existed during the day in both the PBL (median ~ 11 pptv) and
 465 the FT (median ~ 4 pptv) over the Southeast U.S. during the NOMADSS 2013 summer field

466 study. The ground HONO sources did not significantly contribute to the HONO budget in the
467 PBL above the minimum measurement heights of 300 m. HONO budget analysis suggests
468 that photolysis of particulate nitrate was the major volume HONO source (~69%), while the
469 sum of known NO_x-related reactions a minor HONO source (~19%) in the low-NO_x
470 background air masses. HONO was not a significant daytime OH precursor in the PBL away
471 from the ground surface; however, HONO was an important intermediate product of
472 photolysis of particulate nitrate in the renoxification process. Up to several tens pptv of
473 HONO were observed in power plant plumes and urban plumes during the day, mostly
474 produced *in situ* from precursors including NO_x and pNO₃. No significant night-time HONO
475 accumulation was observed in the nocturnal residual layer and the free troposphere, due to
476 low levels of NO_x and specific aerosol surface area.

477

478 **Acknowledgements**

479 This research is funded by National Science Foundation (NSF) grants (AGS-1216166, AGS-
480 1215712, and AGS-1216743). We would like to acknowledge operational, technical, and
481 scientific support provided by NCAR, sponsored by the National Science Foundation. The
482 data are available in our project data archive
483 (http://data.eol.ucar.edu/master_list/?project=SAS). Any opinions, findings, and conclusions
484 or recommendations expressed in this paper are those of the authors and do not necessarily
485 reflect the views of NSF.

486

487 **References**

- 488 Acker, K., Moller, D., Wieprecht, W., Meixner, F. X., Bohn, B., Gilge, S., Plass-Dulmer, C.,
489 and Berresheim, H.: Strong daytime production of OH from HNO₂ at a rural mountain site,
490 *Geophys. Res. Lett.*, 33, Artn L02809, 10.1029/2005gl024643, 2006.
- 491 Baergen, A. M., and Donaldson, D. J.: Photochemical renoxification of nitric acid on real
492 urban grime, *Environ. Sci. Technol.*, 47, 815-820, 10.1021/es3037862, 2013.
- 493 Burling, I. R., Yokelson, R. J., Griffith, D. W. T., Johnson, T. J., Veres, P., Roberts, J. M.,
494 Warneke, C., Urbanski, S. P., Reardon, J., Weise, D. R., Hao, W. M., and de Gouw, J.:
495 Laboratory measurements of trace gas emissions from biomass burning of fuel types from
496 the southeastern and southwestern United States, *Atmos. Chem. Phys.*, 10, 11115-11130,
497 2010.

498 Carr, S., Heard, D. E., and Blitz, M. A.: Comment on "Atmospheric hydroxyl radical
499 production from electronically excited NO₂ and H₂O", *Science*, 324, 2009.

500 de Gouw, J., and Warneke, C.: Measurements of volatile organic compounds in the earths
501 atmosphere using proton-transfer-reaction mass spectrometry, *Mass Spectrom. Rev.*, 26,
502 223-257, 2007.

503 Du, J., and Zhu, L.: Quantification of the absorption cross sections of surface-adsorbed nitric
504 acid in the 335-365 nm region by Brewster angle cavity ring-down spectroscopy, *Chem.*
505 *Phys. Lett.*, 511, 213-218, 10.1016/j.cplett.2011.06.062, 2011.

506 Elshorbany, Y. F., Kleffmann, J., Kurtenbach, R., Lissi, E., Rubio, M., Villena, G., Gramsch,
507 E., Rickard, A. R., Pilling, M. J., and Wiesen, P.: Seasonal dependence of the oxidation
508 capacity of the city of Santiago de Chile, *Atmos. Environ.*, 44, 5383-5394,
509 10.1016/j.atmosenv.2009.08.036, 2010.

510 Finlayson-Pitts, B. J., and J. N. Pitts, Jr.: *Chemistry of the Upper and Lower Atmosphere:*
511 *Theory, Experiments, and Applications*, Academic Press, San Diego, California, 2000.

512 Flagan, R. C.: Electrical mobility methods for sub-micrometer particle characterization. In
513 *Aerosol Measurement: Principles, Techniques, and Applications*, Third Edition (eds P.
514 Kulkarni, P. A. Baron and K. Willeke), pp339-364, John Wiley & Sons, New York, 2002.

515 George, C., Strekowski, R. S., Kleffmann, J., Stemmler, K., and Ammann, M.:
516 Photoenhanced uptake of gaseous NO₂ on solid-organic compounds: a photochemical
517 source of HONO?, *Faraday Discuss.*, 130, 195-210, 2005.

518 Gierczak, T., Jimenez, E., Riffault, V., Burkholder, J. B., and Ravishankara, A. R.: Thermal
519 decomposition of HO₂NO₂ (peroxynitric acid, PNA): Rate coefficient and determination of
520 the enthalpy of formation, *J. Phys. Chem. A*, 109, 586-596, 2005.

521 He, Y., Zhou, X. L., Hou, J., Gao, H. L., and Bertman, S. B.: Importance of dew in controlling
522 the air-surface exchange of HONO in rural forested environments, *Geophys. Res. Lett.*, 33,
523 2006.

524 Hornbrook, R. S., Blake, D. R., Diskin, G. S., Fried, A., Fuelberg, H. E., Meinardi, S.,
525 Mikoviny, T., Richter, D., Sachse, G. W., Vay, S. A., Walega, J., Weibring, P.,
526 Weinheimer, A. J., Wiedinmyer, C., Wisthaler, A., Hills, A., Riemer, D. D., and Apel, E.
527 C.: Observations of nonmethane organic compounds during ARCTAS - Part 1: Biomass
528 burning emissions and plume enhancements, *Atmos. Chem. Phys.*, 11, 11103-11130,
529 2011a.

530 Hornbrook, R. S., Crawford, J. H., Edwards, G. D., Goyea, O., Mauldin, R. L., Olson, J. S.,
531 and Cantrell, C. A.: Measurements of tropospheric HO₂ and RO₂ by oxygen dilution
532 modulation and chemical ionization mass spectrometry, *Atmos. Meas. Tech.*, 4, 735-756,
533 2011b.

534 Huang, G., Zhou, X., Deng, G., Qiao, H., and Civerolo, K.: Measurements of atmospheric
535 nitrous acid and nitric acid, *Atmos. Environ.*, 36, 2225-2235, 2002.

536 Kaser, L., Karl, T., Yuan, B., Mauldin, R. L. III, Cantrell, C. A., Guenther, A. B., Patton, E.
537 G., Weinheimer, A. J., Knote, C., Orlando, J., Emmons, L., Apel, E., Hornbrook, Shertz,
538 R., S., Ullmann, K., Hall, S., Graus, M., de Gouw, J., Zhou, X., and Ye, C.: chemistry-
539 turbulence interactions and mesoscale variability influence the cleansing efficiency of the
540 atmosphere, *Geophys. Res. Lett.*, 42, doi:10.1002/2015GL066641, 2015.

541 Karl, T., Jobson, T., Kuster, W.C., Williams, E., Stutz, J., Shetter, R., Hall, S.R., Goldan, P.,
542 Fehsenfeld, F., and W. Lindinger, W.: The use of Proton-Transfer-Reaction Mass
543 Spectrometry to Characterize VOC Sources at the La Porte Super Site during the Texas Air
544 Quality Study 2000, *J. Geophys. Res.*, 108, doi: 10.1029/2002JD003333, 2003.

545 Kleffmann, J., Kurtenbach, R., Lorzer, J., Wiesen, P., Kalthoff, N., Vogel, B., and Vogel, H.:
546 Measured and simulated vertical profiles of nitrous acid - Part I: Field measurements,
547 *Atmos. Environ.*, 37, 2949-2955, 2003.

548 Kleffmann, J.: Daytime sources of nitrous acid (HONO) in the atmospheric boundary layer,
549 *Chemphyschem*, 8, 1137-1144, 10.1002/cphc.200700016, 2007.

550 Kurtenbach, R., Becker, K. H., Gomes, J. A. G., Kleffmann, J., Lorzer, J. C., Spittler, M.,
551 Wiesen, P., Ackermann, R., Geyer, A., and Platt, U.: Investigations of emissions and
552 heterogeneous formation of HONO in a road traffic tunnel, *Atmos. Environ.*, 35, 3385-
553 3394, Doi 10.1016/S1352-2310(01)00138-8, 2001.

554 Li, S. P., Matthews, J., and Sinha, A.: Atmospheric hydroxyl radical production from
555 electronically excited NO₂ and H₂O, *Science*, 319, 1657-1660, 2008a.

556 Li, X., Rohrer, F., Hofzumahaus, A., Brauers, T., Haseler, R., Bohn, B., Broch, S., Fuchs, H.,
557 Gomm, S., Holland, F., Jager, J., Kaiser, J., Keutsch, F. N., Lohse, I., Lu, K. D., Tillmann,
558 R., Wegener, R., Wolfe, G. M., Mentel, T. F., Kiendler-Scharr, A., and Wahner, A.:
559 Missing gas-phase source of HONO inferred from Zeppelin measurements in the
560 troposphere, *Science*, 344, 292-296, 2014.

561 Li, Y. Q., Schwab, J. J., and Demerjian, K. L.: Fast time response measurements of gaseous
562 nitrous acid using a tunable diode laser absorption spectrometer: HONO emission source
563 from vehicle exhausts, *Geophys. Res. Lett.*, **35**, 2008b.

564 Maljanen, M., Yli-Pirila, P., Hytonen, J., Joutsensaari, J., and Martikainen, P. J.: Acidic
565 northern soils as sources of atmospheric nitrous acid (HONO), *Soil. Biol. Biochem.*, **67**,
566 94-97, 10.1016/j.soilbio.2013.08.013, 2013.

567 Mauldin, R., Kosciuch, E., Eisele, F., Huey, G., Tanner, D., Sjostedt, S., Blake, D., Chen, G.,
568 Crawford, J., and Davis, D.: South Pole Antarctica observations and modeling results: New
569 insights on HO_x radical and sulfur chemistry, *Atmos. Environ.*, **44**, 572-581, 2010.

570 Monge, M. E., D'Anna, B., Mazri, L., Giroir-Fendler, A., Ammann, M., Donaldson, D. J., and
571 George, C.: Light changes the atmospheric reactivity of soot, *P. Natl. Acad. Sci. USA*, **107**,
572 6605-6609, 2010.

573 Ndour, M., D'Anna, B., George, C., Ka, O., Balkanski, Y., Kleffmann, J., Stemmler, K., and
574 Ammann, M.: Photoenhanced uptake of NO₂ on mineral dust: Laboratory experiments and
575 model simulations, *Geophys. Res. Lett.*, **35**, 2008.

576 Ndour, M., Nicolas, M., D'Anna, B., Ka, O., and George, C.: Photoreactivity of NO₂ on
577 mineral dusts originating from different locations of the Sahara desert, *Phys. Chem. Chem.*
578 *Phys.*, **11**, 1312-1319, 2009.

579 Neuman, J.A., Trainer, M., Brown, S.S., Min, K.-E., Nowak, J.B., Parrish, D.D., Peischl, J.,
580 Pollack, I.B., Roberts, J.M., Ryerson, T.B., and Veres, P.R.: HONO emission and
581 production determined from airborne measurements over the Southeast U.S., *J. Geophys.*
582 *Res.-Atmos.*, **121**, 9237–9250, 2016.

583 Oswald, R., Behrendt, T., Ermel, M., Wu, D., Su, H., Cheng, Y., Breuninger, C., Moravek,
584 A., Mougín, E., Delon, C., Loubet, B., Pommerening-Roser, A., Sorgel, M., Poschl, U.,
585 Hoffmann, T., Andreae, M. O., Meixner, F. X., and Trebs, I.: HONO emissions from soil
586 bacteria as a major source of atmospheric reactive nitrogen, *Science*, **341**, 1233-1235,
587 10.1126/science.1242266, 2013.

588 Oswald, R., Ermel, M., Hens, K., Novelli, A., Ouwersloot, H. G., Paasonen, P., Petaja, T.,
589 Sipila, M., Keronen, P., Back, J., Konigstedt, R., Beygi, Z. H., Fischer, H., Bohn, B.,
590 Kubistin, D., Harder, H., Martinez, M., Williams, J., Hoffmann, T., Trebs, I., and Sorgel,
591 M.: A comparison of HONO budgets for two measurement heights at a field station within
592 the boreal forest in Finland, *Atmos. Chem. Phys.*, **15**, 799-813, 10.5194/acp-15-799-2015,
593 2015.

594 Platt, U., and Stutz, J.: Differential Optical Absorption Spectroscopy: Principles and
595 Applications, Springer, Berlin., 2008.

596 Ramazan, K. A., Syomin, D., and Finlayson-Pitts, B. J.: The photochemical production of
597 HONO during the heterogeneous hydrolysis of NO₂, *Phys. Chem. Chem. Phys.*, 6, 3836-
598 3843, 10.1039/b402195a, 2004.

599 Ramazan, K. A., Wingen, L. M., Miller, Y., Chaban, G. M., Gerber, R. B., Xantheas, S. S.,
600 and Finlayson-Pitts, B. J.: New experimental and theoretical approach to the heterogeneous
601 hydrolysis of NO₂: Key role of molecular nitric acid and its complexes, *J. Phys. Chem. A*,
602 110, 6886-6897, 10.1021/jp056426n, 2006.

603 Reed, C., Evans, M.J., Crilley, L.R., Bloss, W.J., Sherwen, T., Read, K.A., Lee, J.D., and
604 Carpenter, L.J.: Evidence for renoxification in the tropical marine boundary layer, *Atmos.*
605 *Chem. Phys.*, 17, 4081–4092, 2017.

606 Ridley, B., Ott, L., Pickering, K., Emmons, L., Montzka, D., Weinheimer, A., Knapp, D.,
607 Grahek, F., Li, L., Heymsfield, G., McGill, M., Kucera, P., Mahoney, M. J., Baumgardner,
608 D., Schultz, M., and Brasseur, G.: Florida thunderstorms: A faucet of reactive nitrogen to
609 the upper troposphere, *J. Geophys. Res.-Atmos.*, 109, 2004.

610 Shetter, R. E., Cinquini, L., Lefer, B. L., Hall, S. R., and Madronich, S.: Comparison of
611 airborne measured and calculated spectral actinic flux and derived photolysis frequencies
612 during the PEM Tropics B mission, *J. Geophys. Res.-Atmos.*, 108, 2002.

613 Stemmler, K., Ammann, M., Donders, C., Kleffmann, J., and George, C.: Photosensitized
614 reduction of nitrogen dioxide on humic acid as a source of nitrous acid, *Nature*, 440, 195-
615 198, 10.1038/nature04603, 2006.

616 Stemmler, K., Ndour, M., Elshorbany, Y., Kleffmann, J., D'Anna, B., George, C., Bohn, B.,
617 and Ammann, M.: Light induced conversion of nitrogen dioxide into nitrous acid on
618 submicron humic acid aerosol, *Atmos. Chem. Phys.*, 7, 4237-4248, 2007.

619 Stein, A. F., Draxler, R. R., Rolph, G. D., Stunder, B. J. B., Cohen, M. D., and Ngan, F.:
620 NOAA's HYSPLIT atmospheric transport and dispersion modeling system. *Bul. Amer.*
621 *Meteorol. Soc.*, 96, 2059-2077, 10.1175/BAMS-D-14-00110.1, 2015.

622 Stutz, J., Alicke, B., and Neftel, A.: Nitrous acid formation in the urban atmosphere: Gradient
623 measurements of NO₂ and HONO over grass in Milan, Italy, *J. Geophys. Res.-Atmos.*,
624 107, Artn 8192, 10.1029/2001jd000390, 2002.

625 Stutz, J., Oh, H. J., Whitlow, S. I., Anderson, C., Dibbb, J. E., Flynn, J. H., Rappengluck, B.,
626 and Lefer, B.: Simultaneous DOAS and mist-chamber IC measurements of HONO in
627 Houston, TX, *Atmos. Environ.*, 44, 4090-4098, 2010.

628 Su, H., Cheng, Y. F., Oswald, R., Behrendt, T., Trebs, I., Meixner, F. X., Andreae, M. O.,
629 Cheng, P., Zhang, Y., and Poschl, U.: Soil Nitrite as a Source of Atmospheric HONO and
630 OH Radicals, *Science*, 333, 1616-1618, 10.1126/science.1207687, 2011.

631 Trentmann, J., Andreae, M. O., and Graf, H. F.: Chemical processes in a young biomass-
632 burning plume, *J. Geophys. Res.-Atmos.*, 108, 2003.

633 VandenBoer, T. C., Brown, S. S., Murphy, J. G., Keene, W. C., Young, C. J., Pszenny, A. A.
634 P., Kim, S., Warneke, C., de Gouw, J. A., Maben, J. R., Wagner, N. L., Riedel, T. P.,
635 Thornton, J. A., Wolfe, D. E., Dube, W. P., Ozturk, F., Brock, C. A., Grossberg, N., Lefer,
636 B., Lerner, B., Middlebrook, A. M., and Roberts, J. M.: Understanding the role of the
637 ground surface in HONO vertical structure: High resolution vertical profiles during
638 NACHTT-11, *J. Geophys. Res.-Atmos.*, 118, 10155-10171, 2013.

639 VandenBoer, T. C., Markovic, M. Z., Sanders, J. E., Ren, X., Pusede, S. E., Browne, E. C.,
640 Cohen, R. C., Zhang, L., Thomas, J., Brune, W. H., and Murphy, J. G.: Evidence for a
641 nitrous acid (HONO) reservoir at the ground surface in Bakersfield, CA, during CalNex
642 2010, *J. Geophys. Res.-Atmos.*, 119, 9093-9106, 10.1002/2013JD020971, 2014.

643 VandenBoer, T. C., Young, C. J., Talukdar, R. K., Markovic, M. Z., Brown, S. S., Roberts, J.
644 M., and Murphy, J. G.: Nocturnal loss and daytime source of nitrous acid through reactive
645 uptake and displacement, *Nature Geosci.*, 8, 55-60, 2015.

646 VandenBoer, T.C., Brown, S.S., Murphy, J.G., Keene, W.C., Young, C.J., Pszenny, A.A.P.,
647 Kim, S., Warneke, C., Gouw, Joost de, Maben, J.R., Wagner, N.L., Riedel, T.P., Thornton,
648 J.A., Wolfe, D.E., Dube, W.P., Ozturk, F., Brock, C.A., Grossberg, N., Lefer, B., Lerner,
649 B., Middlebrook, A.M., and Roberts, J.M.: Understanding the role of the ground surface in
650 HONO vertical structure: High resolution vertical profiles during NACHTT-11, *J.*
651 *Geophys. Res.-Atmos.*, 118, 10,155–10,171, doi:10.1002/jgrd.50721, 2013.

652 Villena, G., Kleffmann, J., Kurtenbach, R., Wiesen, P., Lissi, E., Rubio, M. A., Croxatto, G.,
653 and Rappengluck, B.: Vertical gradients of HONO, NO_x and O₃ in Santiago de Chile,
654 *Atmos. Environ.*, 45, 3867-3873, 2011.

655 Wong, K. W., Oh, H. J., Lefer, B. L., Rappengluck, B., and Stutz, J.: Vertical profiles of
656 nitrous acid in the nocturnal urban atmosphere of Houston, TX, *Atmos. Chem. Phys.*, 11,
657 3595-3609, 2011.

658 Wong, K. W., Tsai, C., Lefer, B., Haman, C., Grossberg, N., Brune, W. H., Ren, X., Luke,
659 W., and Stutz, J.: Daytime HONO vertical gradients during SHARP 2009 in Houston, TX,
660 Atmos. Chem. Phys., 12, 635-652, 2012.

661 Wong, K. W., Tsai, C., Lefer, B., Grossberg, N., and Stutz, J.: Modeling of daytime HONO
662 vertical gradients during SHARP 2009, Atmos. Chem. Phys., 13, 3587-3601, 2013.

663 Wu, C., and Yu, J.Z.: Evaluation of linear regression techniques for atmospheric applications:
664 the importance of appropriate weighting, Atmos. Meas. Tech., 11, 1233–1250, 2018.

665 Ye, C. X., Zhou, X. L., Pu, D., Stutz, J., Festa, J., Spolaor, M., Cantrell, C., Mauldin, R. L.,
666 Weinheimer, A., and Haggerty, J.: Comment on "Missing gas-phase source of HONO
667 inferred from Zeppelin measurements in the troposphere", Science, 348,
668 10.1126/science.aaa1992, 2015.

669 Ye, C. X., Gao, H. L., Zhang, N., and Zhou, X.: Photolysis of nitric Acid and nitrate on
670 natural and artificial surfaces, Environ. Sci. Technol., 50, 3530-3536, 2016a.

671 Ye, C. X., Zhou, X. L., Pu, D., Stutz, J., Festa, J., Spolaor, M., Tsai, C., Cantrell, C., Mauldin,
672 R. L., Campos, T., Weinheimer, A., Hornbrook, R. S., Apel, E. C., Guenther, A., Kaser, L.,
673 Yuan, B., Karl, T., Haggerty, J., Hall, S., Ullmann, K., Smith, J. N., Ortega, J., and Knote,
674 C.: Rapid cycling of reactive nitrogen in the marine boundary layer, Nature, 532, 489-491,
675 2016b.

676 Ye, C., Zhang, N., Gao, H., and Zhou, X.: Photolysis of particulate nitrate as a source of
677 HONO and NO_x, Environ Sci Technol, DOI: 10.1021/acs.est.7b00387, 2017.

678 Young, C.J., Washenfelder, R.A., Roberts, J.M., Mielke, L.H., Osthoff, H.D., Tsai, C.,
679 Pikelnaya, O., Stutz, J., Veres, P.R., Cochran, A.K., VandenBoer, T.C., Flynn, J.,
680 Grossberg, N., Haman, C.L., Lefer, B., Stark, B., Martin, G., Gouw, Joost de., Gilman, J.B.,
681 Kuster, W.C., and Brown, S.S.: Vertically Resolved Measurements of Nighttime Radical
682 Reservoirs in Los Angeles and Their Contribution to the Urban Radical Budget, Environ.
683 Sci. Technol., 46 (20), 10965–10973, 2012.

684 Zhang, N., Zhou, X., Shepson, P. B., Gao, H., Alaghmand, M., and Stirm, B.: Aircraft
685 measurement of HONO vertical profiles over a forested region, Geophys. Res. Lett., 36,
686 Artn L15820,10.1029/2009gl038999, 2009.

687 Zhang, N., Zhou, X., Bertman, S., Tang, D., Alaghmand, M., Shepson, P. B., and Carroll, M.
688 A.: Measurements of ambient HONO concentrations and vertical HONO flux above a
689 northern Michigan forest canopy, Atmos. Chem. Phys., 12, 8285-8296, 2012.

690 Zhou, X., Civerolo, K., Dai, H., Huang, G., Schwab, J., and Demerjian, K.: Summertime
691 nitrous acid chemistry in the atmospheric boundary layer at a rural site in New York State,
692 *J. Geophys. Res.*, *107*, doi:10.1029/2001JD001539, 2002.

693 Zhou, X., Gao, H., He, Y., Huang, G., Bertman, S. B., Civerolo, K., and Schwab, J.: Nitric
694 acid photolysis on surfaces in low-NO_x environments: Significant atmospheric
695 implications, *Geophys. Res. Lett.*, *30*, Artn 2217, 10.1029/2003gl018620, 2003.

696 Zhou, X., Zhang, N., TerAvest, M., Tang, D., Hou, J., Bertman, S., Alaghmand, M., Shepson,
697 P. B., Carroll, M. A., Griffith, S., Dusanter, S., and Stevens, P. S.: Nitric acid photolysis on
698 forest canopy surface as a source for tropospheric nitrous acid, *Nature Geosci.*, *4*, 440-443,
699 10.1038/NGEO1164, 2011.

700 Zhu, C. Z., Xiang, B., Zhu, L., and Cole, R.: Determination of absorption cross sections of
701 surface-adsorbed HNO₃ in the 290-330 nm region by Brewster angle cavity ring-down
702 spectroscopy, *Chem. Phys. Lett.*, *458*, 373-377, 2008.

703

704

705 Table 1. Measurements from the NOMADSS 2013 summer study used in this analysis.

Parameters	Instrument	Time Resolution	Detection Limit	Accuracy	References
HONO	LPAP	200 s	1 pptv	20%	(1, 2)
pNO₃	LPAP	360 s	2 pptv	30%	(1, 2, 3)
HNO₃	LPAP	20 min	2 pptv	30%	(1, 2, 3)
NO	CI	1 s	20 pptv	10%	(4)
NO₂	CI	1 s	40 pptv	15%	(4)
O₃	CI	1 s	100 pptv	5%	(4)
OH	SICIMS	30 s	*5×10 ⁴	30%	(5, 6)
HONO	DOAS	60 s	~ 30 pptv	20%	(7)
Photolysis Frequencies	CAFS	6 s		10-15%	(8)
Surface area density	SMPS/UHSAS	65 s/1 s		20%	(9)
VOCs	PTRMS	15 s		20%	(10, 11)
VOCs/organic nitrates	TOGA	20 s		20%	(12)

706 *in molecules cm⁻³

707 LPAP: long-path absorption photometric (LPAP) systems

708 CI: 4-channel chemiluminescence instrument

709 SICIMS: selected-ion chemical-ionization mass spectrometer

710 DOAS: Differential Optical Absorption Spectroscopy

711 CAFS: Charged-coupled device Actinic Flux Spectroradiometer

712 SMPS: Scanning Mobility Particle Sizer

713 UHSAS: Ultra-High Sensitivity Aerosol Spectrometer

714 PTRMS: Proton Transfer Reaction Mass Spectrometry

715 TOGA: Trace Organic Gas Analyzer

716 References: (1) Zhang et al., 2012; (2) Ye et al., 2016b; (3) Huang et al., 2002; (4) Ridley et

717 al., 2004; (5) Hornbrook et al., 2011b; (6) Mauldin et al., 2010; (7) Platt and Stutz, 2008;

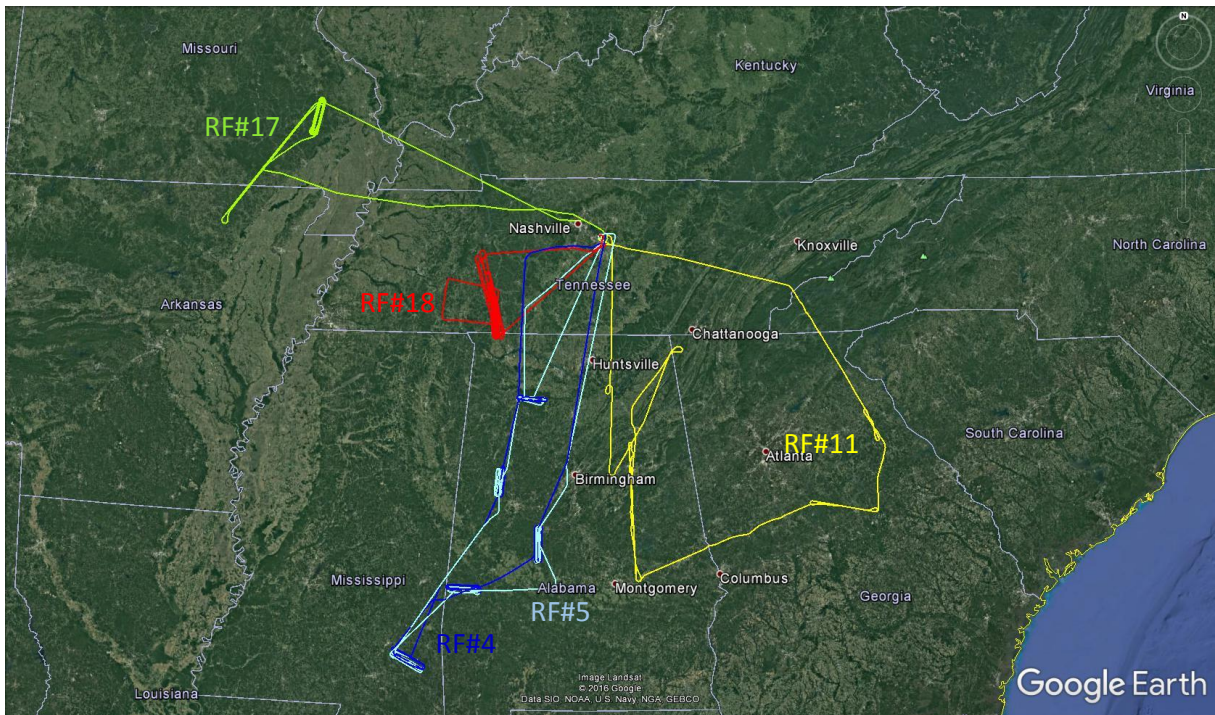
718 (8) Shetter et al., 2002; (9) Flagan, 2011; (10) Karl et al., 2003; (11) de Gouw and

719 Warneke, 2007; (12) Hornbrook et al., 2011a.

720 Table 2. Data statistics for HONO, NO_x and pNO₃ measurements both in the PBL and the FT
 721 from the five Southeast U.S. research flights during the NOMADSS 2013 summer field study.
 722 The statistics analysis is based on 1-min NO_x data, 3-min HONO data and 6-min pNO₃ data.
 723

		HONO, pptv	NO _x , pptv	pNO ₃ , pptv
PBL	Range	3.1 – 34.4	81 – 1774	9 – 186
	Mean ± SD	11.2 ± 4.3	316 ± 182	76 ± 45
	Median	10.3	279	66
	N	356	904	121
FT	Range	1.3 - 15.2	<10 – 582	3 – 179
	Mean ± SD	5.6 ± 3.4	94 ± 53	35 ± 39
	Median	4.2	92	15
	N	157	655	46

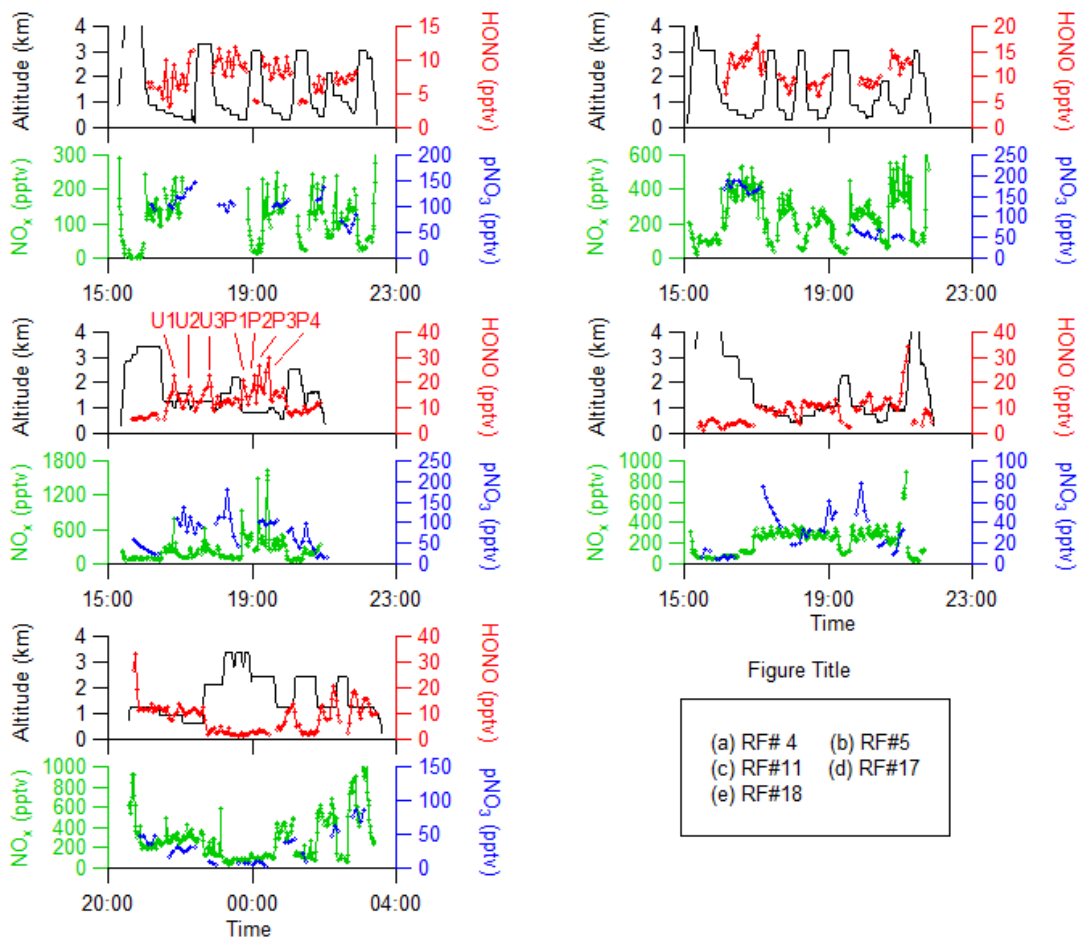
724



725

726 Figure 1. Flight tracks in the Southeast US during the NOMADSS 2013 summer study. The
 727 flight start time and end time in UTC (= EDT+4) are: RF#4 (blue): 15:12 and 22:30, June 12,
 728 2013; RF#5 (light blue): 15:04 and 21:52, June 14, 2013; RF#11 (yellow): 15:20 and 21:02,
 729 June 29, 2013; RF#17 (green): 15:07 and 21:57, July 11, 2013; RF#18 (red): 20:32, July 12,
 730 2013, and 03:37, July 13, 2013.

731

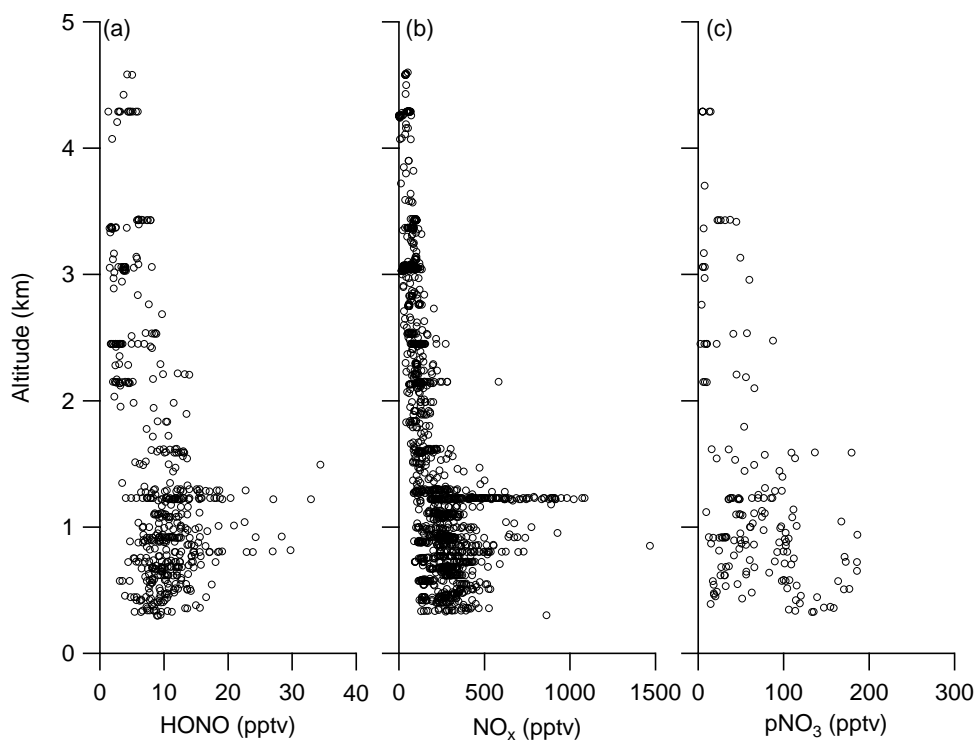


732

733

734 Figure 2. Time series of altitude, HONO, NO_x and pNO₃ in five flights (RF #4, RF #5, RF
 735 #11, RF #17 and #18) in the Southeast US during the NOMADSS 2013 summer study. In RF
 736 #11, the plumes U1 and U3 were from Birmingham, AL; the plume U2 was from
 737 Montgomery, AL; the plumes P1-P3 were from a power plant in Monroe County, GA; and the
 738 plume P4 was from a power plant in Putnam country, GA.

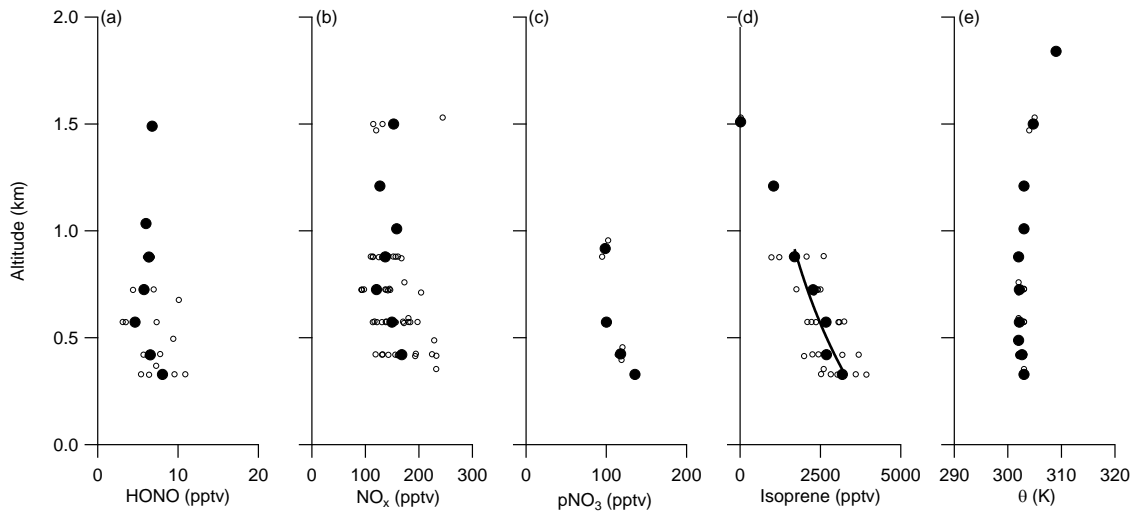
739



740

741 Figure 3. Vertical distributions of concentrations of HONO (a), NO_x (b), and pNO₃ (c) in the
742 five selected flights in the Southeast US during the NOMADSS 2013 summer study.

743

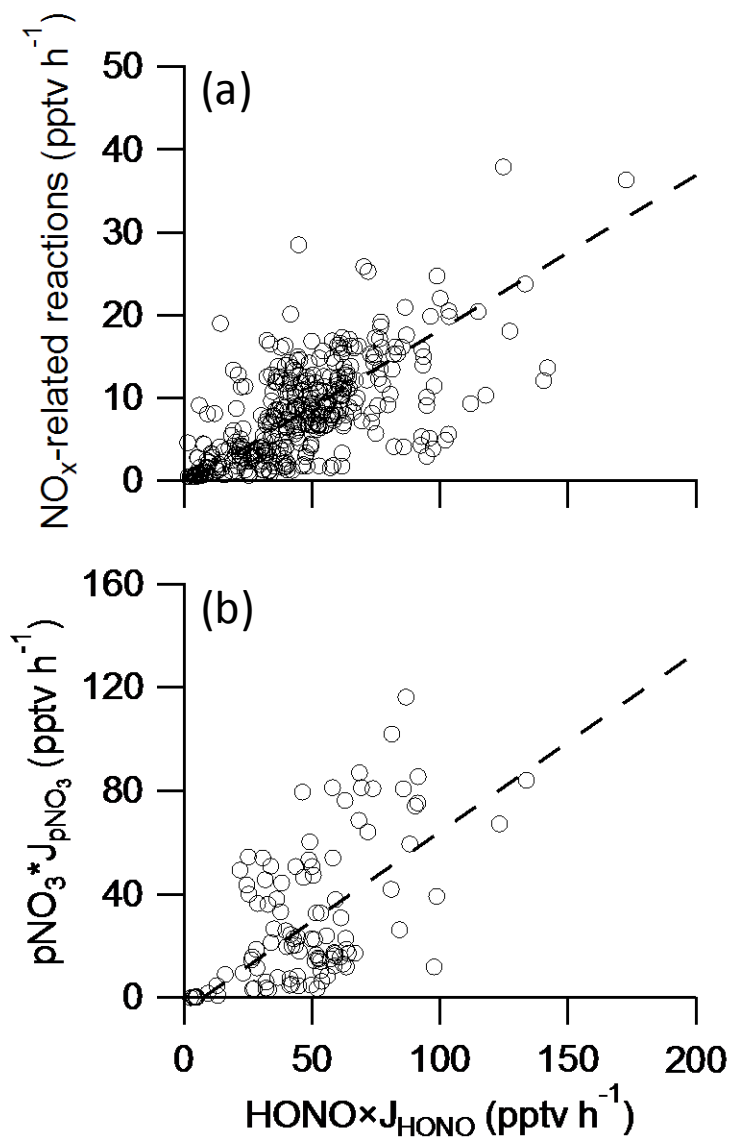


745

746 Figure 4. Vertical distributions of concentrations of HONO (a), NO_x (b), pNO₃ (c), isoprene
 747 (d) and potential temperature (e) in the PBL during the first race-track of RF#4 from 11:00 –
 748 12:15 LT (16:00 – 17:15 UTC), June 12, 2013. The small open circles represent the 1-min
 749 data points, the large solid circles the mean values for each race-track measurement altitude.

750 The line in (d) is the best fit of (Eq. 1) to the isoprene data: $C = 4700e^{-h/0.895}$, $r^2 = 0.93$.

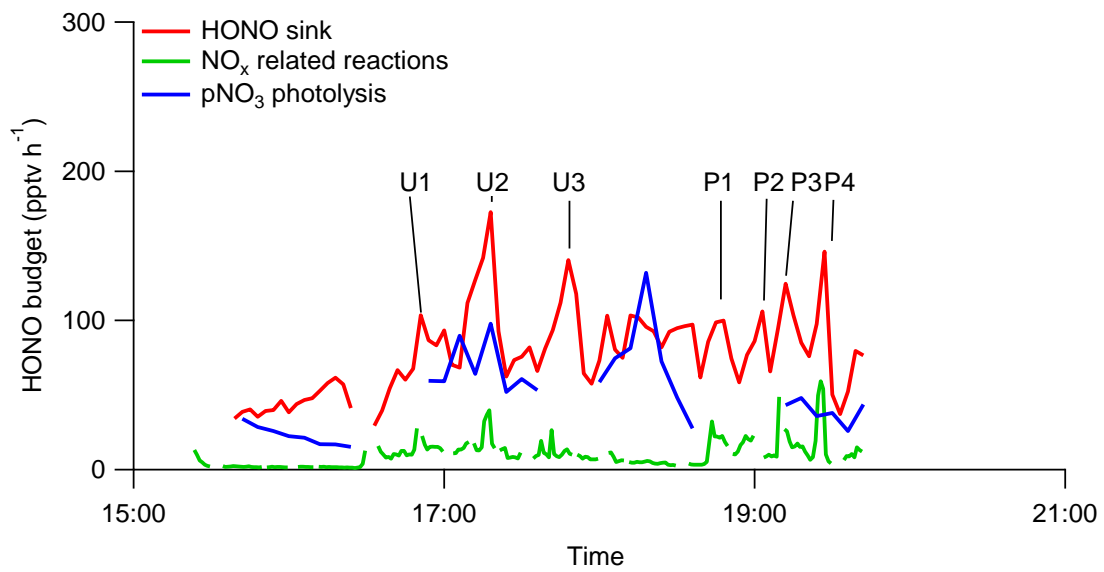
751



752

753 Figure 5. Correlation analysis of main HONO sink (“HONO×J_{HONO}”) with contribution from
 754 NO_x related reactions (a) and with contribution from particulate nitrate photolysis,
 755 pNO₃×J_{pNO₃} (b) in the southeast US during the NOMADSS 2013 summer study. The line
 756 represents the Deming least-squares regression (Wu and Yu, 2018) ($r^2=0.40$, intercept = -0.51
 757 and slope = 0.19 for Figure 6a; $r^2=0.34$, intercept = -5.0 and slope = 0.69 for Figure 6b).

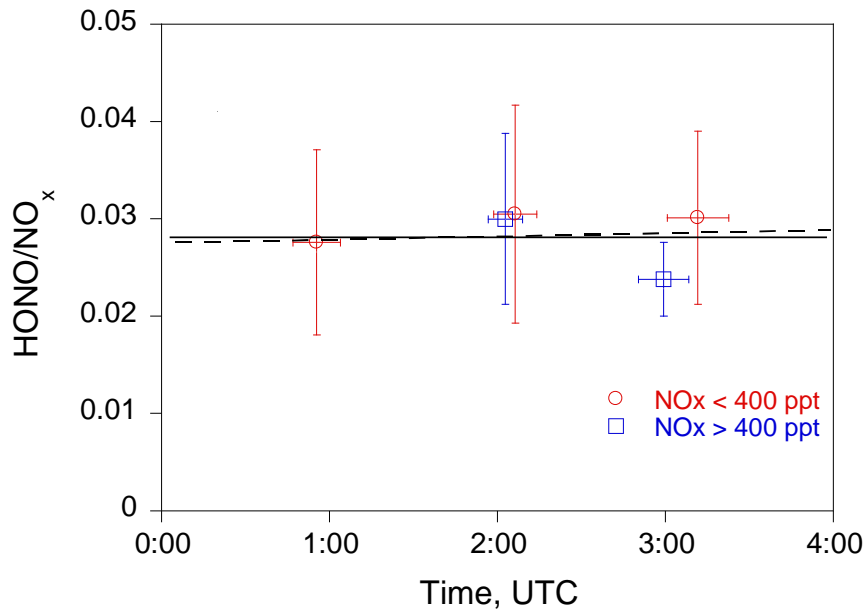
758



760

761 Figure 6. HONO budget analysis in RF #11 in the Southeast US during the NOMADSS 2013
 762 summer study. “HONO sink” is the HONO loss rate contributed by photolysis and the
 763 reaction of HONO with OH radicals, “NO_x related reactions” is the sum of HONO production
 764 rates from all known NO_x reactions, and “pNO₃ photolysis” is the HONO production rate
 765 from photolysis of pNO₃. The calculations are based on 1-min NO_x data, 3-min HONO data
 766 and 6-min pNO₃ data.

767



768

769 Figure 7. The evolution of HONO/NO_x ratio in the nocturnal boundary layer during the
 770 RF#18. The red circles and blue squares are the median HONO/NO_x values under the
 771 conditions of NO_x ≤ 400 pptv and NO_x > 400 pptv, respectively. The horizontal bars indicate
 772 the averaging time periods and the vertical bars the one standard deviation of HONO/NO_x
 773 ratios. The solid line is the least squared fit to the data, and the dashed line indicates a slope
 774 of $3 \times 10^{-4} \text{ hr}^{-1}$. The sunset time at the sampling location was 0:40 UTC.

775